Computer Communications 215 (2024) 29–40

Contents lists available at ScienceDirect

Computer Communications

journal homepage: www.elsevier.com/locate/comcom

Contactless wheat foreign material monitoring and localization with passive RFID tag arrays

Erbo Shen [a,e], Weidong Yang [b,*], Xuyu Wang [c], Shiwen Mao [d]

[a] Henan Key Laboratory of Grain Photoelectric Detection & Control, Henan University of Technology, ZhengZhou, Henan, China
[b] College of Information Science & Engineering, Henan University of Technology, Zhengzhou, China
[c] Knight Foundation School of Computing & Information Sciences, Miami, FL, USA
[d] Department of Electrical and Computer Engineering, Auburn University, Auburn, AL, USA
[e] Kaifeng university, Kaifeng, Henan, China

ARTICLE INFO

Keywords:
Radio Frequency Identification (RFID)
Radio frequency sensing
Foreign material recognition
Localization

ABSTRACT

In the early stage of harvesting, transportation, and storage, the grain could be mingled with clods from the field, metal pieces from aging machines, and other objects of foreign material, which will greatly influence the grain quality and food security. In this paper, we propose a novel radio frequency (RF) sensing system termed TagSee, which utilizes passive RFID tag arrays to sense the objects buried in wheat. The goal is to simultaneously sense the presence of foreign materials, locate their locations in the 3D space and sense their types, to automatically monitor the stored grain. Specifically, we use RFID received signal strength (RSS) and phase as features for foreign material detection. To design the TagSee system, we first introduce a sensing space division method. Then, an Euclidean Distance Ratio (EDR) algorithm and a heuristic method are proposed to achieve high localization success accuracy. A multi-class SVM method is used to sense different materials properties based on the impact of different foreign materials on signal features. Experimental results show that TagSee can effectively detect foreign materials in stored grain and achieve a centimeter-level localization success accuracy, and can recognize four types of objects in grain.

1. Introduction

As the rapid increase of global population, the demand for food will be doubled by year 2050 [1]. Grain quality is one of the key indicators related to food security. Through the stages of grain harvesting, transportation, and storage, the grain could be contaminated by foreign materials such as clod and rock from the field, metal and rubber pieces from various equipment due to aging, which will greatly affect the grain quality. Generally, the foreign materials are manually sorted by farmers in the early stage of grain harvest, which is time-consuming and laborious. Recently, radio frequency identification (RFID) based radio frequency (RF) sensing has attracted great attention due to the low cost, easy deployment, and high sensing accuracy. Successful applications of RFID-based sensing include indoor scene sensing and localization [2–5], material identification [6,7], human pose monitoring [8–10], moisture sensing [11,12], and human vital sign monitoring [13]. Inspired by the above applications, we propose TagSee for simultaneous detection and localizing foreign material in stored gain using commercial off-the-shelf (COTS) RFID devices. The goal is to quickly identify foreign materials and remove them from stored grain. TagSee utilizes the phase and received signal strength (RSS) data from RFID signals that propagate through the grain for material identification and localization. Both phase and RSS are provided by many commodity RFID devices. TagSee works well with a small 8 MHz bandwidth. Specifically, *TagSee design is motivated by the key observation that the multi-path propagation and absorption effects on the RSS and phase of received RFID signal will be affected by the presence of foreign materials in wheat. More important, different materials have varying effects on RFID signals.* Therefore, the changes of RFID signals may reflect the properties of the foreign materials. Besides, the presence of foreign materials will produce multi-path effects, and the received signal is actually the result of the superposition of multiple signals, which is related to the distance. According to the electromagnetic wave theory, when the wireless signal encounters a foreign material, some signals are reflected and refracted, while the others are absorbed by the material. Thus, the received signal will vary with different absorption rates, which is greatly related to material properties. This feature will be exploited for foreign material classification in TagSee system.

In particular, wheat is considered as a sensing medium that can be penetrated by electromagnetic waves, while common static foreign

* Corresponding author.
E-mail addresses: shenerbo4@stu.haut.edu.cn (E. Shen), yangweidong@haut.edu.cn (W. Yang), xuywang@fiu.edu (X. Wang), smao@ieee.org (S. Mao).

https://doi.org/10.1016/j.comcom.2023.12.019
Received 9 June 2023; Received in revised form 16 December 2023; Accepted 18 December 2023
Available online 21 December 2023

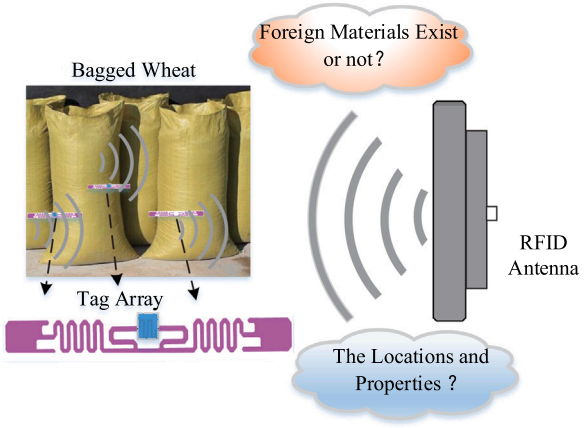

Fig. 1. Sense foreign materials using RFID tag arrays in NLOS.

materials in wheat (e.g., screws, clods, etc.) are used as sensing targets without tag attached on. The proposed TagSee system consists of three steps. The first step is to sense the foreign materials for the presence in medium. The second is to sense the locations of foreign materials in space (i.e., a three-dimensional space). The third is to sense the types of foreign materials in medium. The schematic diagram of the system is shown in Fig. 1. Tag arrays are deployed on the sensing area, and the space is filled with wheat medium. The medium can be penetrated by wireless signals to ensure that foreign materials can be sensed. Two reading antennas are deployed vertically above each of the two tag arrays. This sensing scheme can be also applied to other penetrable medium (e.g., liquid, soil and other grain).

To sum up, some RFID based sensing technologies use coarse-grained RSS to sense moving target [4,14,15], and some put the tags on the targets to sense them when they are in Line Of Sight (LOS) scene [16–20]. However, in many applications, the sensing targets are unknown and invisible, i.e., whether a target existing is unknown, and its location and properties are also unknown in Non Line Of Sight (NLOS), which poses a big challenge. This paper proposes a contactless method to sense the location and types of multiple unknown targets when the targets are buried in the medium with NLOS.

The main contributions of this work are summarize in the following.

- To the best of our knowledge, the proposed TagSee system is the first contactless system to simultaneously locate foreign materials and sense their properties with cheap COTS RFID devices. More important, TagSee can sense static targets without tags be attached on, even when the targets are unknown in non-line-of-sight (NLOS) scenarios.
- In NLOS scenarios, TagSee uses two tag arrays to achieve effective detection of foreign materials. Specifically, we propose a novel Euclidean Distance Ratio (EDR) algorithm and a heuristic method to achieve higher localization success accuracy.
- We develop a prototype of TagSee to verify the effectiveness of the proposed approach. The experimental results demonstrate that TagSee can effectively detect foreign objects and achieve a centimeter-level location success accuracy.

The remainder of this paper is organized as follows. We present the related work in Section 2, and preliminaries study in Section 3. Section 4 introduces the design of the TagSee system. Section 5 presents the experimental evaluation of TagSee. Conclusions are drawn in Section 6.

2. Related work

The existing foreign materials detection methods generally include ultrasonic detection [21,22], optical detection [23,24], nuclear detection [25,26], and electromagnetic wave detection [27,28]. For the ultrasonic detection methods, they have the advantages of stronger ability to penetrate material, and it is easy to achieve an automatic detection. However, these methods need couplant, which will pollute the detection sample. Optical detection methods (e.g., X-ray) can perform nondestructive detecting on the internal structure and defects of targets, and are widely used in many applications. While the special detection equipment could achieve the detection purpose, the equipment is expensive and difficult to be deployed. The advantage of the nuclear methods is that the detection depth is greater. However, these methods require strict protective measures, and the equipment is complex and costly, which cannot meet the requirements for online detection. The electromagnetic wave methods have the advantages of flexible, fast and high accuracy, which is one of the most promising detection technologies with non-destructive and non-contact. They also have been used in many application devices, but this kind of equipment is very expensive, bulky, inconvenient to be deployed, and difficult to be applied on a large scale.

Radio Frequency (RF) such as radar and Wi-Fi is a type of wireless sensing technologies widely used in Internet of Things (IoT) [29,30]. Among RF sensing technologies, Radio Frequency Identification (RFID), as one of the key technologies in the field of IoT, becomes an important wireless sensing method due to its low cost, easy deployment, and high sensing accuracy. RFID has been used in indoor scene sensing and localization [2,31–35], material identification [6,7,36], human body monitoring [16,19,20,37], moisture sensing [11,12,38] and other IoT fields [39–45].

Specifically, RFID tags have been used for location [5] and material identification [6] related to our work. For indoor scene sensing, some systems use Received Signal Strength (RSS) as a feature to achieve a coarse-grained indoor localization. The LANDMARC system [3] and the work [46] show that RFID is a viable and cost-effective candidate for indoor location sensing, both of which use RSS as the feature to estimate the location by active RFID tag. The works [4,33] employ passive RFID to achieve a real-time RFID-based location system and indoor symbolic localization, respectively. GSOS-ELM [47] introduces an RFID indoor positioning algorithm based on the Glowworm Swarm Optimization (GSO) with a semi-supervised online sequential extreme learning machine (SOS-ELM). However, the above all technologies locate the targets by using the RSS feature, which is a coarse grain feature that cannot be used to identify materials inside the medium. Moreover, the works [3,46] use active RFID tags for sensing, which increases the difficulty of the deployment. By contrast, the phase as a fine-grained sensing feature, is used for more accurate positioning. The works [48,49] both use phase difference to achieve better accuracy, while [48] proposes a fast approach for dynamic object localization based on the fusion of the RFID phase and the laser information. Also, [49,50] propose a 3-D localization scheme based on phase, which both achieve a relatively satisfactory accuracy. The above works all attach the tags to the target to estimate its location. However, the robustness of these systems are challenged due to the sensitivity of the phase to the environment.

For material identification, the works [6,7,51] use phase difference as a main feature to identify material types when a tag is attached on the target. Work [51] proposes a Reflected Amplitude Feature(RAF) method to sense four types of material with the best accuracy of 95%, and the work [7] employs a Dynamic Time Warping (DTW) algorithm [52] to identify the material type by evaluating the similarity of the estimated material pattern with those material patterns in the database. More importantly, the work [6] uses both RSS and phase to identify the types of material, which is related to our work. However, for the above works, the tag must be attached on the target when system is working, and it can only identify the liquid (e.g., milk, soil and water). Moreover, most of the above works take the moving objects as sensing targets, for RFID signal are sensitive to moving objects, and are not so effective for the static objects (e.g., wheat foreign materials).

In this paper, we design TagSee, a system that can identify the foreign material types and position simultaneously with cheap COTS RFID devices, which can help people quickly find foreign material and remove them in NLOS environment. Unlike existing systems that attach tag to the target by extracting the reflectivity and permeability parameters for sensing the target, TagSee exploits the phase and RSS changes when the signal penetrates inside a target for material identification and localization. We believe this work introduces a new direction for performing material identification and localization with COTS RFID devices.

3. Preliminaries study

3.1. RSS based sensing

For a wireless electromagnetic environment in the free space, the RSS of RFID Tag is expressed by Eq. (1),

$$P_R = P_T(\frac{\lambda \sqrt[2]{G_R}\sqrt[2]{G_T}}{4\pi d})^2, \tag{1}$$

where P_R and P_T represent the powers of the receiver and the transmitter, respectively, G_R and G_T represent the antenna gains of the receiver and the transmitter, respectively, and d represents the distance between the receiver and the transmitter. According to Eq. (1), the power of the receiver depends on the distance d if the transmission power and the antenna gain are constants. Thus, the distance d is one of the factors that affect RSS. In addition, we use Eq. (2) to express RSS in the wheat when there is no foreign material as following,

$$RSS(d) = RSS(d_0) - 10 \times \gamma \times log_{10}(\frac{d}{d_0}) + S_{0,\sigma}, \tag{2}$$

where $RSS(d)$ represents RSS (with the unit of decibel) with the signal propagation distance from tag to receiver antenna, d_0 denotes vertical distance which is the shortest distance between tag and receiver in this system, and $RSS(d_0)$ represents RSS when the distance is d_0, which is a constant. γ represents the path loss factor ($0 < \gamma < 1$). $S_{0,\sigma}$ represents Gaussian noise (e.g., the mean value is 0, and the variance is σ). The RSS difference method is used to eliminate Gaussian noise. The propagation path of the signal is defined as d' when there is foreign material in wheat, and d' represents the superimposed path of the signal after being interfered by foreign material. Then, ΔRSS is expressed by,

$$\Delta RSS = RSS(d) - RSS(d') \tag{3}$$

$$= 10 * \gamma log_{10}(\frac{d'}{d}). \tag{4}$$

Eq. (3) shows that RSS is related to the distance d' and d. Recall that d' and d represent the signal propagation path with and without foreign material in wheat, respectively. $\frac{d'}{d}$ should be 1 if foreign material does not affect the propagation path of the signal, and ΔRSS should be 0. However, the observation shows ΔRSS is a number greater than zero. Thus, we can conclude that $d' > d$, i.e. foreign material indeed changes the propagation path of the tag signal, which is the reason why we can used RSS to sense foreign material.

We conduct the experiment to show how ΔRSS changes by the object, where the object is placed between tag and RFID antenna, and the object is moved away from tag by step. We observe the RSS changes and Fig. 2 illustrates how the RSS changes with the distance from tag to object. The results indirectly show that the RSS is changed by the superimposed the d'.

In addition, for the object with high absorptivity, part of the signal is absorbed by material and lost in the form of heat, which also causes RSS changes. Thus, RSS is one feature can be used for sensing material in wheat. Moreover, we will discuss the other feature that can be also used in sensing foreign material, which is a fine-grained feature phase.

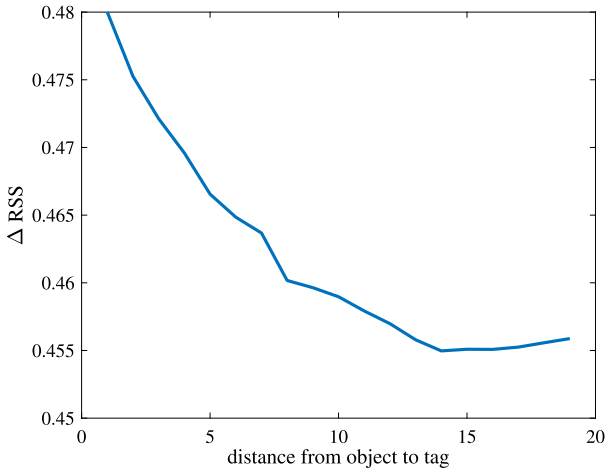

Fig. 2. ΔRSS varies with the distance from tag to object.

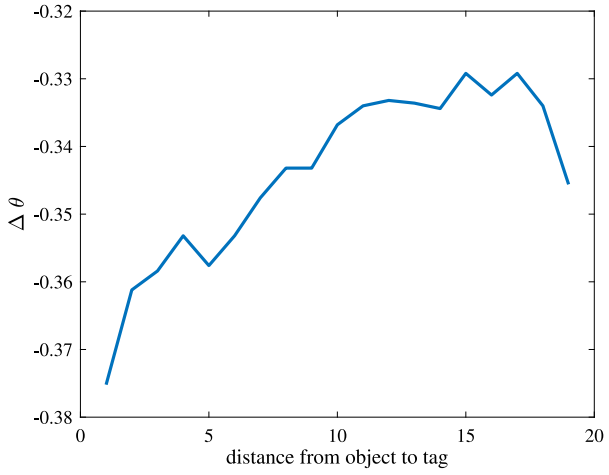

Fig. 3. $\Delta\theta$ varies with the distance from tag to object.

3.2. Phase based sensing

Let λ represent the wavelength of signal in medium. Then the phase θ can be expressed as the following Eq. (5),

$$\theta(d) = (\frac{2\pi}{\lambda} \times 2d + \theta_T + \theta_R + \theta_{Tag}) mod 2\pi, \tag{5}$$

where θ_T, θ_R, and θ_{Tag} represent the phase intrinsic offsets caused by back-scattering of the transmitting antenna, the receiving antenna, and the RFID tag, respectively [6]. These offsets will be different for different hardware, but they will not change with the distance d in indoor environment. Therefore, they can be eliminated by phase difference as Eq. (6),

$$\Delta\theta = \theta(d) - \theta(d') \tag{6}$$

$$= \frac{2\pi}{\lambda} \times 2\Delta d + 2k\pi, \tag{7}$$

where $\Delta d = d - d'$, k represents an integer, $\theta(d)$ and $\theta(d')$ represent phases with and without foreign material, respectively. If the foreign material does not change the path of the tag signal, i.e. $d' = d$, there should be $\Delta\theta = 0$ or $\Delta\theta = 2k\pi$. We conduct the same experiment as Section 3.1, and Fig. 3 also supports the above ideas that the phase can be used to sense the foreign materials because the propagation path d' is changed by the foreign materials.

Figs. 2 and 3 illustrated that both RSS and θ are changed by the object in sensing space, and they are related with the object's position.

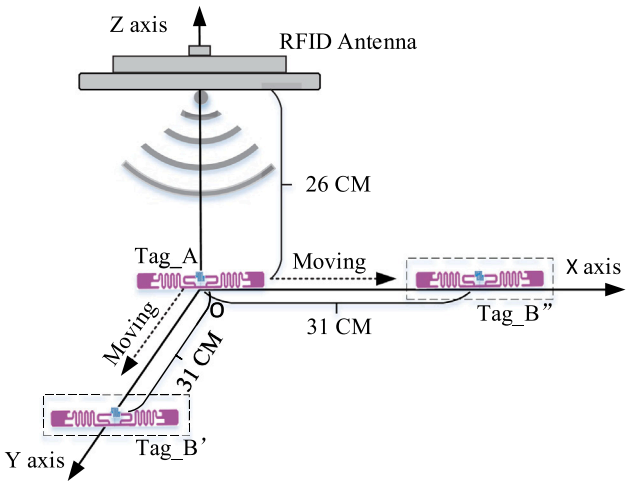

Fig. 4. tag A is fixed, tag B moves along X and Y axis respectively.

In addition, the material properties (absorptivity and reflectivity) also affect propagation path of tag signal, which is a complex physical process that is difficult to be expressed by a mathematical model. Thus, machine learning methods are considered to sense material properties, which will be presented in Section 4.4.

3.3. Electromagnetic coupling between RFID tags

Electromagnetic coupling is also called mutual inductance coupling. The current change in a circuit will affect the other circuit due to the mutual inductance coupling between the two circuits [53]. It is concluded in [54] that when the tag spacing is less than 30 mm, the derived mutual impedance expression is applied to the frequency offset calculation with the error range in 1.6 MHz–7.3 MHz. Also, the authors [55] consider that the coupling effect has a greater impact on the phase measurement when the distance between two tags is less than 40 cm.

For TagSee, the location success accuracy will be influenced if the RFID tags are too far apart, while the performance of the system will decline if the spacing between two tags are too small due to the coupling. In other words, the deployment distance of tags cannot be too dense or too sparse. Thus, there should be an optimal deployment scheme, which enables TagSee to maximize the recognition accuracy while maintaining its performance. To verify the coupling effect between two tags, the following experiments are conducted, as shown in Fig. 4.

First, we put RFID Tag_A and Tag_B together. Fixing Tag_A, we move Tag_B along the X axis and Y axis, respectively, while recording the changes in the feature vectors (RSS, θ) of Tag_A and Tag_B with the increase distance from 0 cm to 31 cm. Fig. 4 shows the direction of the movement of the Tag_B, where Tag'_B and Tag''_B represent two different movement directions for Tag_B, respectively.

As deployed in Fig. 4, the changes of RSS and θ for Tag_A and Tag_B are recorded as Tag_B is moving. Also, Fig. 5(a) and Fig. 5(b) show that RSS and phase θ of Tag_A vary with the movement of Tag_B. For phase θ, the effect of the coupling on Tag_A almost disappears when Tag_B moves to 24 cm along X axis, and 18 cm along the Y axis, respectively. For RSS, the effect of coupling on Tag_A almost disappears when Tag_B moves to 22 cm along X axis, and 17 cm along the Y axis, respectively. In Table 1, to reduce the impact of electromagnetic coupling on the system, the spacing between tags along X and Y axes should be greater than the minimum uncoupling-distance. The above conclusion is utilized as benchmark to deploy the tag arrays with proper distances. It will help design a more reasonable tag array in the latter section.

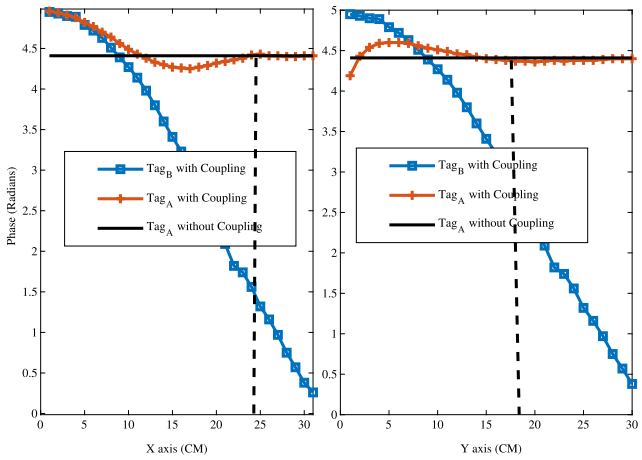

(a) tag_A phase changes as tag_B moving.

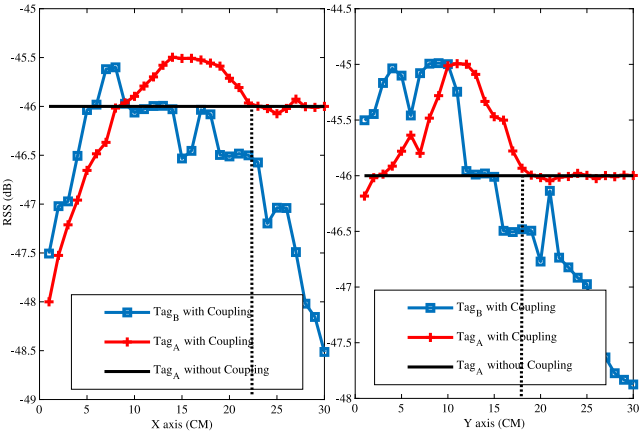

(b) tag_A RSS changes as tag_B moving.

Fig. 5. RSS and θ from Tag_A keep unchanged when Tag_B moves far away.

Table 1
The minimum distance of tag non-coupling effect in two directions.

Minimum uncoupling-distance	
X-axis direction	Y-axis direction
24 cm	18 cm
22 cm	17 cm

3.4. Influence of multi-path

According to the electromagnetic wave theory, when the signal passes through two different medium, it will reflect and refract at the interface between the two medium. Because the properties of foreign materials are different from the medium, the signal transmission mode will change at their interface, resulting in multi-path phenomenon. Thus, the multi-path is the result of multiple transmissions and reflections of signals in space. Although the multi-path in some works (e.g., [6,56]) is regarded as the noise or the interference, for this work, in the internal sensing space, the multi-path occurred in medium is due to the presence of foreign materials. Specifically, for the presence of foreign materials, the multi-path occurs inside the medium, including signal reflection, transmission, refraction, etc. Thus, the feature RSS and θ of the signal will change. Based on the preliminary study in the previous section, the multi-path occurred inside the medium can be used to sense foreign materials. However, there is a multi-path

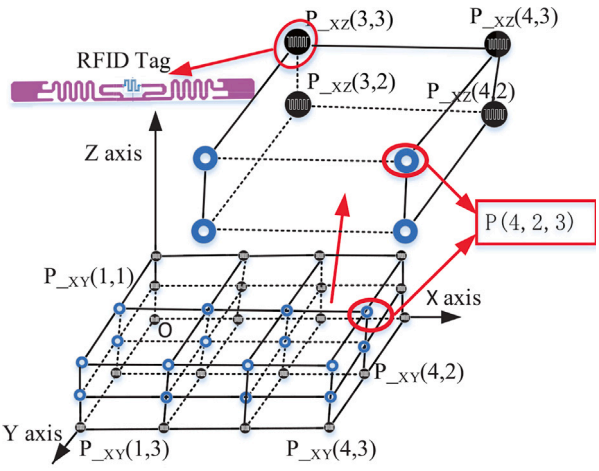

Fig. 6. The sensing space is marked by a 3D grid according to the two tag arrays deployed on the XOY and XOZ plains.

occurred outside regarded as an interference signal, which affects the performance of TagSee. It can be mitigated by adjusting the equipment deployment and using the wave absorbing sponge, in which the multi-path impact can be reduced.

4. TagSee system design

In order to sense foreign materials in NLOS scenarios, we first mark the 3D sensing space by a 3D grid according to the two tag arrays deployed on the sides of the 3D space. Then, a foreign material detection and localization algorithm based on the concept of EDR will be proposed. Then, a heuristic method will be used to re-locate the foreign material if the EDR method fails. Finally, a multi-class SVM method is used to sense the properties of the foreign materials.

4.1. Partition the sensing space

TagSee deploys multiple RFID tags in the two adjacent planes (i.e., the XOY plane and the XOZ plane) to form two tag arrays. As shown in Figs. 6 and 7, the two tag arrays are deployed in plane XOY and XOZ (the two sides of the 3D sensing space), respectively. Then the internal region of the sensing space can be marked by a virtual 3D grid, while each grid point's 3D coordinates are given by the 2D coordinates of the corresponding tag on the XOY plan and that on the XOZ plane. A foreign material's location can be represented by the nearest grid point in the 3D space.

As the example in Fig. 6 shows, a 4×3 tag array is deployed on the XOY plane and the other 4×3 tag array on the XOZ plane. Then the 3D sensing space can be marked by a $4 \times 3 \times 3$ grid. Let $P(X, Y, Z)$ represent the $3D$ coordinate of a grid point (marked by the blue circles in Fig. 6), and $P_{XY}(X, Y)$ and $P_{XZ}(X, Z)$ represent the $2D$ coordinates of the deployed tags on the XOY and XOZ planes, respectively. For instance, the grid point $P(4, 2, 3)$ is determined by the tags at $P_{XY}(4, 2)$ and $P_{XZ}(4, 3)$. TagSee can locate foreign material by determining the coordinates of the nearest grid point $P(X, Y, Z)$. Although the above method can detect the spatial coordinates of the foreign material, the localization accuracy is limited by the density of tags in the two arrays, while the density may affect the electromagnetic coupling between the tags. Due to the above limitations, Tagsee can only obtain the target's approximate location. We believe that it is sufficient for the sensing system that we can still easily locate and remove objects in practice. To quantify the accuracy of localization, we represent the localization of foreign objects in the form of probability, which will be discussed in Section 4.2.1.

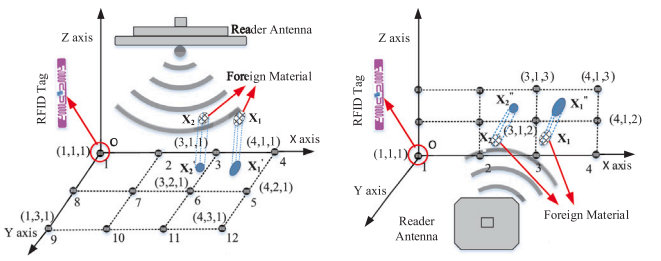

Fig. 7. Project object onto the XOY and XOZ planes using the EDR algorithm.

4.2. Sensing with the Euclidean distance ratio algorithm

The RSS and phase θ from RFID tags are collected as features in the form of vectors (RSS, θ) by TagSee. Both RSS and θ are affected by the distance d, foreign materials, as well as their properties. It has been shown that the features are sufficiently sensitive to the foreign material in preliminaries study section. In this section, we will show that the feature vector (RSS, θ) can be used for sensing the location and type of the foreign material using the proposed algorithm.

4.2.1. Design of the Euclidean distance ratio algorithm

When there is foreign material between the RFID tag and reader antenna, its collected feature vector (RSS, θ) will be affected. We find that the feature vector from a tag will have a larger change if the foreign material is closer to the tag. More important, we leverage Euclidean distance to measure the change of the feature vector before and after foreign material are presence in sensing space. The distance between two points of $V_1(x_1, y_1, z_1)$ and $V_2(x_2, y_2, z_2)$ in the 3D space is given by $d_{Eu} = \sqrt{(x_1 - x_2)^2 + (y_1 - y_2)^2 + (z_1 - z_2)^2}$. TagSee collects the feature vectors (RSS, θ), with and without foreign material in the medium (i.e., wheat), from a tag i, which are denoted by $V_0(i)(RSS\_0, \theta\_0)$ and $V_1(i)(RSS\_x, \theta\_x)$, respectively. We calculate the distance between two vectors $V_0(i)$ and $V_1(i)$ as $d_{Eu}(V_0(i), V_1(i))$, where $d_{Eu}(\cdot, \cdot)$ denotes the Euclidean distance between two feature vectors. Therefore, we define the Euclidean distance ratio (EDR) as follows,

$$EDR(i) = \frac{d_{Eu}(V_0(i), V_1(i))}{|V_0(i)|} \tag{8}$$

$$= \frac{\sqrt{(RSS(i)\_x - RSS(i)\_0)^2 + (\theta(i)\_x - \theta(i)\_0)^2}}{\sqrt{(RSS(i)\_0)^2 + (\theta(i)\_0)^2}}, \tag{9}$$

Then we can identify the tag j with the largest EDR value.

$$\text{tag}(j) = \arg\max_i \{EDR(i)\}, \forall i, i = 1, \ldots, n. \tag{10}$$

Theoretically, the value of $EDR(i)$ should be zero when there is no foreign material in the wheat. Eq. (10) indicates that it is highly likely that tag j is the nearest one to the foreign material. By (8) and (10), the foreign material in the wheat is projected on the tag location (j) whose EDR is the largest.

Taking plane XOY as an example, an array with 4×3 tags are represented as tag i $(i = 1, 2, \ldots, 12)$, as shown in Fig. 7. X_1 represents a foreign material in the space. We can project X_1 onto the XOY plane using the EDR algorithm, by locating X_1 at the grid point $X_1'(4, 2, 1)$ by (10), where the EDR value is the maximum. Similarly, we can also project X_1 onto the XOZ plane at the grid point $X_1''(4, 1, 3)$, which has the maximum EDR. In this way, the foreign material can be projected onto the XOY and XOZ planes at the closest tag using the EDR algorithm. The accuracy of the object projection is presented as a probability. For an $M \times N$ tag array, Eq. (11) and the matrix (12) are used to express the location probability as the following.

$$P_{tag}(i, j) = \frac{EDR(i, j)}{\sum_{i=1}^{M} \sum_{j=1}^{N} EDR(i, j)}, \tag{11}$$

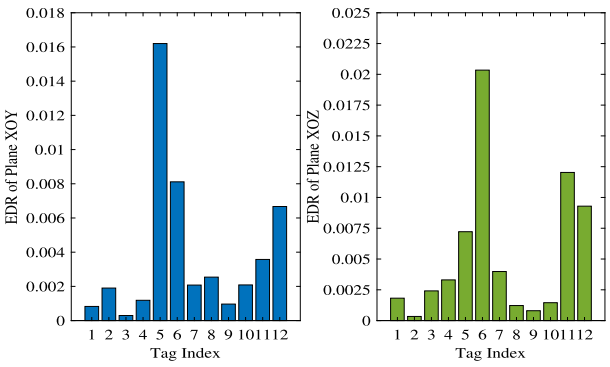

Fig. 8. An example of failed localization of the foreign material. Tag 5 at $P_{XY}(4,2)$ has the highest EDR on the XOY plan and tag 6 at $P_{XZ}(3,2)$ has the highest EDR on the XOZ plane. Since $(x=4)\neq(x'=3)$, we cannot identify a grid point as the location of the foreign material.

$$\begin{bmatrix} P_{tag}(1,1) & \cdots & P_{tag}(1,N) \\ \vdots & \ddots & \vdots \\ P_{tag}(M,1) & \cdots & P_{tag}(M,N) \end{bmatrix}, \tag{12}$$

where $P_{tag}(i,j)$ denotes the possible locations on plane $P_{XY}(i,j)$ or $P_{XZ}(i,j)$; $EDR(i,j)$ denotes the EDR from $tag(i,j)$, and $\sum_{i=1}^{M}\sum_{j=1}^{N} P_{tag}(i,j)=1$. TagSee first determines whether the foreign material exists or not. Then, it obtains the EDRs from all tags, and calculates the weight of each tag's EDR using Eq. (11). The weight represents the probability of the tag projecting onto the plane. In Section 5.4, we use heat map to represent the location probability where the objects are presence in using matrix (12).

4.2.2. Spatial localization of foreign materials

Intuitively, to locate the object position, there are two steps. First, we project the foreign material onto 2-D planes XOY and XOZ to obtain two location points, respectively. Second, the virtual intersection of the two points in space is defined as the spatial position of the object.

An $M\times N$ tag array in the XOY plane and an $M\times L$ tag array in the XOZ plane can form an $M\times N\times L$ grid space. The grid points are labeled with coordinates $P(X,Y,Z)$. Denote the origin point O as $P(1,1,1)$. Assume that the target X presents a foreign material in the wheat with a feature vector $V(RSS\_x,\theta\_x)$. TagSee first uses the EDR algorithm to obtain the $EDR(X)$ values of all the tags in two arrays. Then, the projected locations are obtained in the form of $P_{XY}(x,y)$ and $P_{XZ}(x',z)$. The spatial location coordinates $P(x,y,z)$ can be obtained if $x'=x$, and consequently the location of the foreign material can be determined. For example, the foreign material X is projected on the two planes with $P_{XY}(4,2)$ and $P_{XZ}(4,3)$, as shown in Fig. 6. Then X is located to be near the grid point $P(4,2,3)$, and X can be removed by hand next. However, we cannot find a grid point if $x'\neq x$, which is considered as localization failure. It can be seen in Fig. 8 that there are two abnormal EDR values corresponding to tag 5 and tag 6 in the XOY and XOZ planes, respectively. The coordinates of the two corresponding tags are $P_{XY}(4,2)$ and $P_{XZ}(3,2)$, respectively. Note that $x'\neq x$, we cannot find a grid point in this case and the foreign material is not located.

To improve the success accuracy of localization, we propose a heuristic method. When the localization fails, TagSee seeks for other possible locations. The EDR values from all tags will be rearranged as follows: (i) For plane XOY, $EDR_{XY}(1) > EDR_{XY}(2) > \cdots > EDR_{XY}(j) > \cdots$; (ii) For plane XOZ, $EDR_{XZ}(1) > EDR_{XZ}(2) > \cdots EDR_{XZ}(k) > \cdots$. The above arrangements indicate the possibility of projected locations on the two planes, from large to small. If localization fails for the first time, i.e., there is not a grid point satisfying both $EDR_{XY}(1)$ and $EDR_{XZ}(1)$, TagSee continues to search down the two lists to find a pair of EDR values that satisfy the $x'=x$ condition,

Algorithm 1 Online Relocation Estimation: Heuristic method

Input: Tag feature vectors $V(RSS,\theta)$
Output: Location $P(x,y,z)$ of X
EDR algorithm for all tags feature vectors: $EDR_{XY}(i)$, $EDR_{XZ}(i)$
Rearranged $EDR_{XY}(i)$, $EDR_{XZ}(i)$ of two planes
for j=1:TagNumber **do**
  Plane XOY:Project the $EDR_{XY}(i)$, achieve coordinate $P_{XY}(x,y)$
  Plane XOZ:Project the $EDR_{XZ}(i)$, achieve coordinate $P_{XZ}(x',z)$
  if $(x=x')$ **then**
    return result $P(x,y,z)$
  else
    Project $EDR_{XZ}(i+1)$ on Plane XOZ
    if $(x=x')$ **then**
      return result $P(x,y,z)$
    else
      Project $EDR_{XY}(i+1)$ on Plane XOY
      if $(x=x')$ **then**
        return result $P(x,y,z)$
      end if
    end if
  end if
  return failure
end for
There is no a crossing-point, and the localization fails

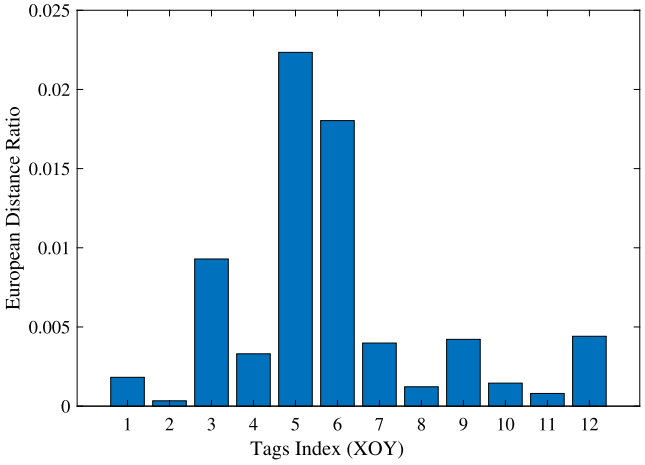

Fig. 9. EDRs when there are two foreign materials.

which then provides the estimated location of the foreign material. The algorithm process is shown in Algorithm 1, which can improve the location success accuracy. We will verify its performance in the latter section.

4.3. Multiple foreign materials sensing

When there are multiple foreign materials in wheat, $EDR(i)$ can be used for determining the number of object. Taking the plane XOY as an example, as shown in Fig. 7. When two objects X_1 and X_2 are placed in sensing space, $EDR(i)$ is obtained for all tags in plane XOY. Fig. 9 shows that there are two abnormal tags of tag(5) and tag(6) on plane XOY, which are the projection locations of X_1 and X_2, respectively. Therefore, TagSee can determine the number of foreign materials by counting the abnormal EDRs.

However, there are two cases in which the TagSee cannot accurately count foreign materials. The first is that the distances between foreign materials are too close to count. Second, when there are too many

foreign materials or even more than the number of tags, they cannot be accurately counted. For the first case, the TagSee considers these materials as one foreign material, where people may remove two or more foreign objects in one place in a time. For the second case, we can increase the number of tags in the tag array to count more foreign materials in larger space.

4.4. Properties recognition using multi-class SVM method

TagSee collects the vectors (RSS, θ) from RFID tags to identity foreign material. We leverage a multi-class SVM method to identify materials, such as clods and rock blocks brought in during grain harvest, and plastic belts and metal screws falling due to the aging machines.

For a multi-class SVM method, M Support Vector Machines (SVM) are constructed for M classes, and each SVM separates data of one class from other classes. During the test, the class with the largest output value of the decision function is considered as the class of the test sample. The ith SVM can be obtained by the following optimization problem,

$$\min_{w^i, b^i, \xi^i} \ \frac{1}{2}(w^i)^T w^i + C \sum_{t=1}^{N} \xi_t^i. \tag{13}$$

The constraint condition can be expressed by,

$$\begin{cases} (w^i)^T \ O(X_t) + b^i \geq 1 - \xi_t^i \\ (w^i)^T \ O(X_t) + b^i \geq -1 + \xi_t^i \\ \xi_t^i \geq 0, \end{cases} \tag{14}$$

where the subscript t represents the index of samples, N represents the number of samples, the superscript $i \in \{1, 2, \ldots, M\}$ denotes the class index, w and b are weight parameters of the hyperplane, respectively, ξ is Lagrange multiplier, C is a constant number, and $O(X_t)$ is the optimal hyperplane function of sample X. Thus, a total of M binary SVMs can be trained by solving the quadratic programming problems with n variables. The Ref. [57] provides the detailed derivation process. In this paper, we set $M = 4$ (types of foreign material). The decision function is given by

$$f(X_{new}) = \underset{i \in \{1, \ldots, M\}}{argmax} \left\{ \sum_{X_t \in s_v} y_t \cdot \alpha_t^i \cdot \kappa\langle X_t, X_{new} \rangle + b^i \right\}, \tag{15}$$

where s_v denotes the support vectors, $\kappa\langle \cdot, \cdot \rangle$ represents the kernel function, $\kappa\langle X_t, X_{new} \rangle$ represents the inner product of X_t and X_{new}, α is dimensional weight vector, y is augmented vector of samples. Thus, if a new sample data X_{new} achieves the largest $f(x_{new})$, then X_{new} will be predicted to be in class i. The following six steps can be used for multiple materials classification.

Step 1: TagSee collects feature vectors of all RFID tags with and without foreign materials in medium. Note that the tag feature vector only needs to be collected once when there is no foreign material, and will never be collected again, thus it is once for all in this step.

Step 2: The training and testing datasets are established. 70% of them are selected for training, while 30% are selected for testing randomly.

Step 3: The data input is normalized to the range of [0, 1].

Step 4: We select the kernel function and parameters of the multi-class SVM. In this paper, we consider the Gaussian radial basis function (RBF) as the kernel function.

Step 5: The SVM is trained using data sets samples, where we use LIBSVM toolbox to implement material classification [57].

Step 6: Then, the trained model in Step 4 could be employed for the identification of foreign materials.

As the number of tags deployed in the environment increases, the feature vectors collected by TagSee will increase dramatically. This will lead to a lower operating efficiency and recognition accuracy. In the worst case, the SVM training function does not converge quickly, because there is a large amount of redundant data, which interferes with the accuracy of the system. Therefore, in order to reduce the interference data and improve the system efficiency and recognition accuracy, we propose to exploit the EDR algorithm to simplify the redundant tags. Specifically, the tags feature vectors with higher EDR values are selected to train the SVM model.

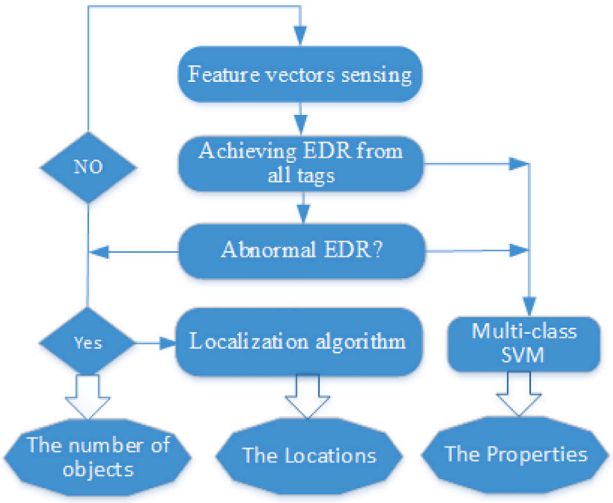

Fig. 10. The system flow chart.

In this section, we present the TagSee design, and the system flow chart is summarized in Fig. 10, which represents three functions of TagSee, i.e., the amount, the location and the properties of foreign material. Next, we will verify the above algorithms in Section 5.

5. Experiment verification

5.1. TagSee setup

As shown in Fig. 11, the sensing space with the size 116 × 56 × 26 cm^3, is made of organic glass (poly-methyl methacrylate). This material can mitigate the impact of the interference on the system, because poly-methyl methacrylate has a minimal interference with electromagnetic waves, which can almost be ignored. The sensing space is filled with grain. TagSee is implemented with two passive RFID tag arrays (with the Alien 9640 tag with Higgs 3 chips) on the XOY plane and the XOZ plane, respectively. Each array consists of 4 × 3 tags. A reader with two Laird2 S9028 PCR RFID antennas is used to query the tags, and a tablet computer with Windows 10 system is used to process the collected data. RFID tag arrays are placed at the bottom and one side of sensing space, and the tag arrays on both sides form a virtual grid to mark the sensed 3D space holding the grain. Four types of foreign materials are used, including clod, plastic, rock, and metal screws, which are common in stored grain. To verify the system's sensing performance for objects with different sizes, Fig. 12 shows two sets of four types of foreign materials with sizes about 2.5 × 3.5 cm^2 and 1 × 2.5 cm^2. Note that we only taken four representative materials as sensing targets, but in practice, the majority of foreign materials are one of these four categories. Therefore, the four types chosen in this experiment are representative and reasonable.

5.2. Foreign material detection

In this section, we verify the sensitivity of EDR values to foreign material. We first measure $V_0(i)(RSS\_0, \theta\_0)$ with the clean grain samples. Next, we place clod, metal, rock, and plastic in the grain, respectively, and measure the corresponding $V_1(i)(RSS\_0, \theta\_0)$ values.

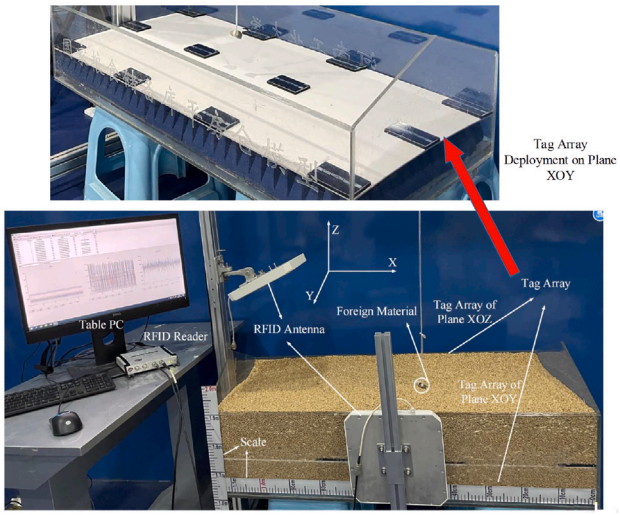

Fig. 11. Deployment of the experimental system.

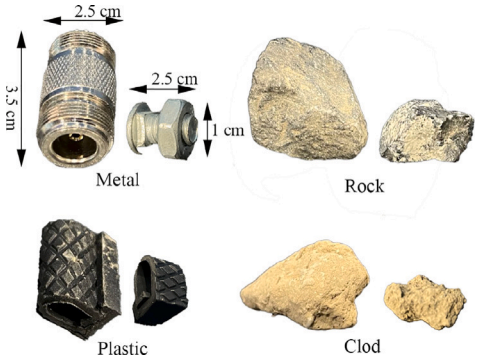

Fig. 12. Four types of objects with large/small size that common in grain storage.

To facility a fair comparison, we place the foreign material in the same position each time. Note that there is only one foreign material in the sensing space in each experiment. Finally the EDR value for each tag is computed as in (8). Take plane XOY as example, data is collected when the foreign material is placed above tag 4. Fig. 13 shows the EDR values for the four types of materials with large and small sizes, respectively. Fig. 13(a)–(d) represent the EDRs of metal, rock, clod and plastics, respectively, where Metal_L, Metal_S denote large and small metal objects respectively, and the same definition is set for rock, clod, plastic. For the large objects with size about 2.5×3.5 cm^2, it is clearly see that the EDR of tag 4 is abnormal since the foreign material is near this tag. Thus, it can be inferred there should be a foreign material in the wheat. However, there are more abnormal EDR in the case of metal, as shown in Fig. 13(a), which does not mean that there are more foreign materials in the wheat. In fact, this is because metals have a strong shielding effect on electromagnetic waves, causing such abnormal EDR values. For smaller objects with sizes about 1×2.5 cm^2, TagSee can sense metal and rock, but for clod and plastic, TagSee fails to sense them. As illustrated in Fig. 13(c) and Fig. 13(d) with red line, there are more than one abnormal EDRs, and they are difficult to distinguish between EDRs in tags. Thus, it can be concluded that TagSee cannot sense plastics and clod with size smaller than 1×2.5 cm^2.

When there may be multiple objects in the grain, we will verify the effectiveness of the multiple foreign materials sensing method mentioned in Section 4.3 as following.

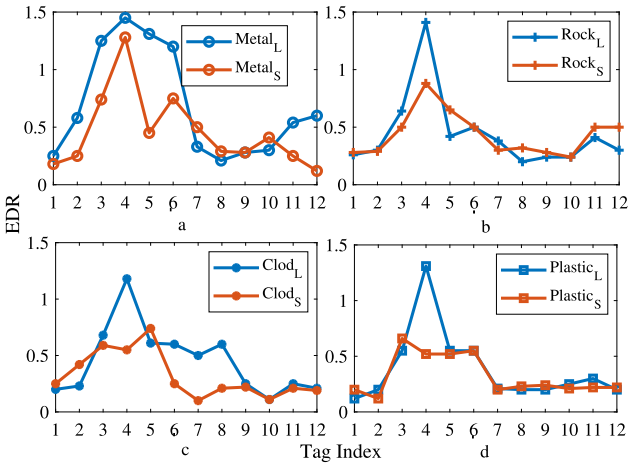

Fig. 13. EDR values for the four types of materials with different sizes.

5.3. Multiple foreign materials sensing

To enable Tagsee to detect multiple objects, it is necessary to obtain the EDR values of all the tags in clean wheat (i.e., without foreign materials). TagSee collects the feature vectors of the tags from clean wheat, it only needs to be collected once. The collected data will be used to compare with the data of the wheat that contains foreign objects. Then, TagSee collects the feature vector $V(RSS, \theta)$ of each tag with foreign materials. As shown in Fig. 14, it indicates the difference of θ and RSS before and after foreign material are present in wheat and air, respectively. Fig. 14(a) represents the RSS that is in air and in wheat when the metal screw is placed. We can see that RSS in wheat changes more greatly than that of θ. By contrast, the phase changes greatly in air, as shown in Fig. 14(b). The above experimental results show that it is easy to sense one foreign material only by observing RSS or θ. The results also indicate that when foreign materials are present in the air, they are easier to be detected than in wheat, because foreign materials have stronger absorption or reflection properties in the air. In addition, due to the weak magnetic medium properties of wheat, signals attenuate more in wheat than in air.

For scenarios with multiple materials in wheat, the foreign materials are placed in the sensing space to observe the changes in EDR. Fig. 15 shows the relation between abnormal EDR and the foreign material numbers using the EDR algorithm, where Fig. 15(a), (b), (c), (d) represent the EDR of tag when {rock}, {rock, plastic},{rock, plastic, clod}, {rock, plastic, clod, metal} are presence in wheat, respectively. In Fig. 15(a) and Fig. 15(b), we can observe that there is one abnormal EDR corresponding to tag 9 and two corresponding to tag 6 and tag 11. Three foreign materials can be observed corresponding to tag 2, tag 3 and tag 9 in Fig. 15(c). However, it is difficult to determine the number of foreign materials from Fig. 15(d). We conclude that TagSee can sense less than three foreign materials easily through a array with 3×4 tags. Also, if there are more foreign materials, we need to use a larger tag array to improve the sensing performance.

5.4. Foreign material localization

5.4.1. Projection onto planes

Section 5.2 validated that TagSee can detect foreign materials in wheat by abnormal values of EDR of tag(i) in plane XOY and tag(j) in plane XOZ, and Eq. (11) illustrated that object's projection position is a probability issue, indicating the possibility of the foreign object being at that position. Thus, we consider using heat map to represent the possibility of an object projected onto the planes. We use linear interpolation to interpolate matrix (12). Fig. 16 shows the possible

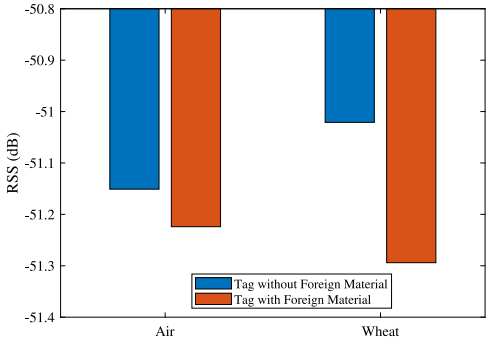

(a) RSS in air and wheat.

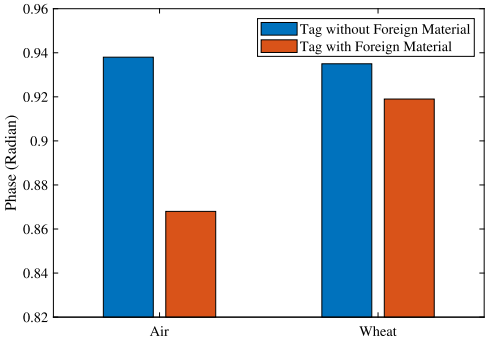

(b) Phase in air and wheat.

Fig. 14. RSS and θ before and after foreign material present.

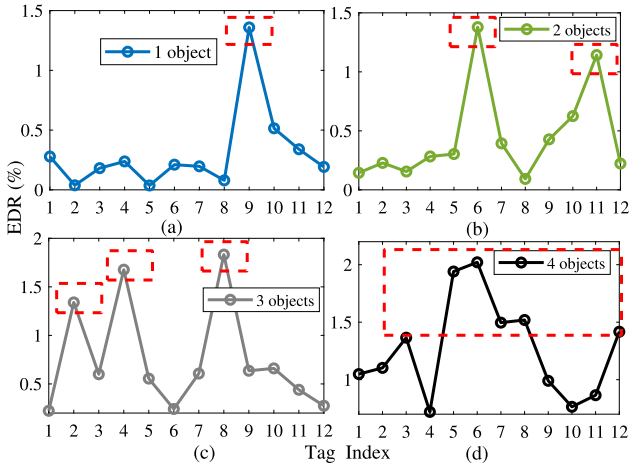

Fig. 15. EDR of multiple foreign materials in wheat.

position that one object's projection on planes, where the intensity of brightness indicates the possibility of object position, and the higher the brightness, the greater the possibility is. Fig. 16(a) and Fig. 16(b) show one object's projection position on plane XOY and XOZ, respectively. Therefore, the most likely projection positions should be $P_{XY}(2,2)$ and $P_{XZ}(2,3)$. Fig. 16(c) and Fig. 16(d) show the smaller object's projection on planes. In Fig. 16(d), we can find that TagSee is difficult to determine the correct projection position because there are two possible positions mixed together. Thus, we conclude that the smaller objects are more difficult to be located using a 3×4 tag array.

Fig. 17 shows the projection of multiple foreign materials on a plane, where Fig. 17(a)- Fig. 17(c) represent the projection on a 3×4 tag array, and Fig. 17(a) represents the projection positions when there are two objects in wheat, which shows that the objects can be easily distinguished. Fig. 17(b) shows the projection positions when two objects are close together, and the projection positions of these two objects are overlapped. Fig. 17(c) shows the projection of three objects, where the projection positions are mixed together, making it more difficult to be distinguished. Fig. 17(d) shows the projection of three foreign objects on a 4×5 tag array, indicating that they can be distinguished clearly using a larger tag array.

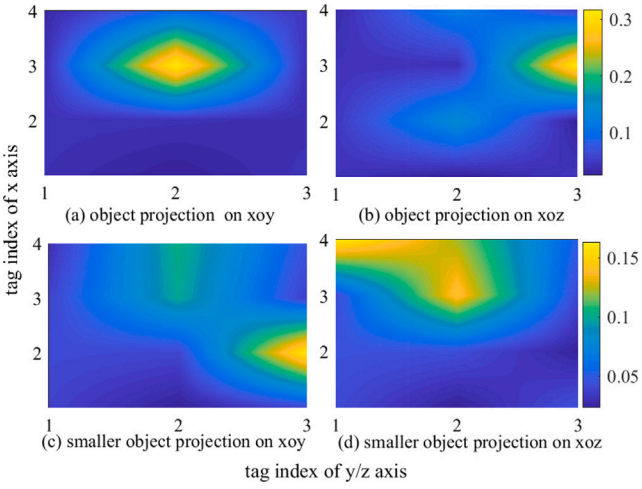

Fig. 16. The objects with different size projection on the plane XOY and XOZ.

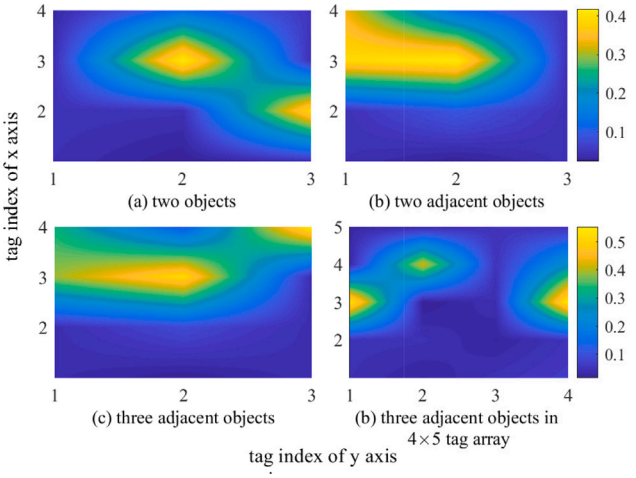

Fig. 17. Projection positions of objects using different number of tag array.

In the following experiment, we present the performance of TagSee using the methods proposed in Section 4.2 when TagSee is working in different medium (air and wheat), and shows the performance when TagSee senses the different type of foreign materials. The foreign materials are randomly placed in the sensing space. TagSee collects RFID tags feature vectors $V(RSS, \theta)$, and 500 data packets are collected for each tag. We repeat the above operations for 50 times to obtain different material feature vectors, and record the coordinates in each experiment. The foreign materials are projected onto planes XOY and XOZ using the EDR algorithm. The projection success accuracy is counted as shown in Table 2, which indicates the success accuracy for projecting foreign material on XOY plane and XOZ planes in medium of air and wheat, respectively. We find that the metal performs the best localization success accuracy of 100%, and the plastic with the worst accuracy of 76%. These findings indicate that TagSee's performance is

Table 2
Success accuracy of projecting various foreign materials on plane XOY and XOZ.

Foreign materials	Air		wheat	
	XOY	XOZ	XOY	XOZ
Metal	100%	100%	100%	100%
Rock	96%	94%	92%	92%
Clod	90%	84%	88%	86%
Plastic	82%	82%	78%	76%

Table 3
Spatial localization success accuracy using heuristic method in air.

Object \ Relocating Times	1	2	3	4
Metal	100%	\	\	\
Rock	92%	96%	\	\
Clod	76%	84%	92%	\
Plastic	70%	80%	88 %	88 %

related to the material's dielectric properties. Specifically, the metal is more sensitive to electromagnetic waves than the other three materials. In addition, the accuracy is better in air medium than that in wheat medium, because there is less interference in the air than that of in the wheat medium. Thus, TagSee's performance is also related to the properties of medium where foreign material exist.

5.4.2. Spatial localization with heuristics method

Tables 3 and 4 represent the spatial location success accuracy using the heuristic method in air and in wheat, respectively. For the plastic in wheat, the initial localization accuracy is only about 70% with 30% failure rate both in air and wheat. The localization success rate in air and wheat increases from 70% to 88% and 84%, respectively using the heuristic method. In addition, the success accuracy in air medium is higher than that in wheat, which again verifies that the localization success accuracy is not only related to the object's properties, but also to the medium in which the object is placed.

We test the TagSee's performance using smaller foreign material in the follows. Intuitively, smaller targets have less absorption and reflection for tag signal, so that there should be less changes in feature vectors $V(RSS, \theta)$ when objects are presence in wheat. To verify the above idea, we performed experiments using smaller size objects as sensing targets in wheat. The results are presented in Table 4, where $Metal_s$, $Rock_s$, $Clod_s$ and $Plastic_s$ denote the smaller sized objects, as shown in Fig. 12. TagSee can effectively locate metal and rock with smaller size. However, for smaller sized clod and plastic, the performance of TagSee is significantly reduced. Therefore, TagSee is more sensitive to objects with properties such as metals and rocks, while it is less sensitive to dry clod and plastics. Essentially, the results are related to the dielectric constant of the objects. Next, we use the multi-class SVM method to identify four types of objects and indirectly verify the results.

5.5. Foreign material recognition

We verify the method proposed in Section 4.4 for sensing the type of material in NLOS scenarios. Data collected in Section 5.2 will be used for training the model. Here, TagSee collects the feature vector $V(RSS, \theta)$ of all RFID tags, consisting of 2 elements RSS and θ, with each tag collecting 500 data packets. There are 12 tags in total. When there are 12 coordinate points in the sensing space, TagSee needs to collect at least $2 \times 500 \times 20 \times 12$ data samples for training and modeling. Fig. 18(a) shows the recognition results using feature vectors from all the RFID tags in XOY and XOZ plane in the medium of wheat. It presents the best accuracy of only 79% for metal recognition, and the worst accuracy of only 69% for plastic, which is not a satisfactory result.

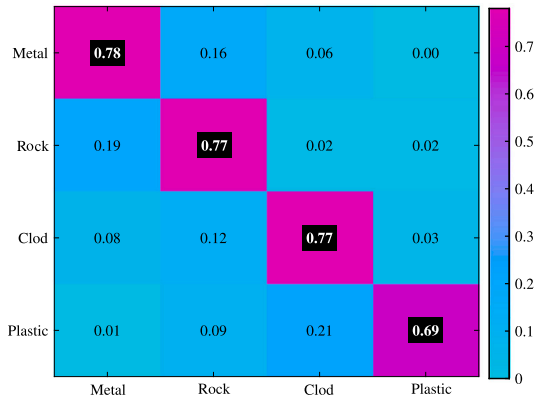

(a) Confusion matrix using all tags feature vectors.

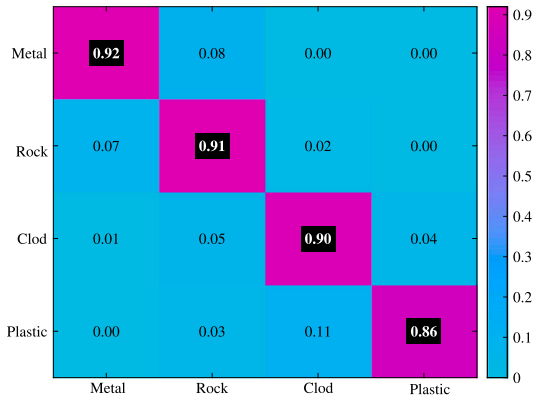

(b) Confusion matrix using 3 tags feature vectors.

Fig. 18. Confusion matrix of foreign material recognition.

In fact, collecting and processing a large amount of data does require more system resources and computational power. At the same time, too much redundant data can lead to a decrease in system performance and increase the cost of data storage and processing. For designing and implementing TagSee, it is necessary to balance the quantity and quality of data. We need to select appropriate sampling methods and algorithms, in order to achieve the best performance and effectiveness. Based on the above idea, we consider selecting some (instead of all) RFID tag feature vectors as samples for training the model. TagSee uses 3 feature vectors with greater EDR values to identify the targets based on the EDR algorithm. In this way, most tags are regarded as the redundant data, which greatly reduces the calculation of the system. The result is shown in Fig. 18(b). The accuracy is improved greatly with the best of 92% for the metal, and the worst of 86% for the plastic in the medium of wheat.

Figs. 18(a) and 18(b) show that metal has the highest recognition rate. This is due to the significant difference in relative dielectric constant between metal and wheat. Generally, the dielectric constant of metal ranges from 8 to 10, while that of wheat is between 3 and 5. Therefore, metal is easier to be identified in wheat. In contrast, plastic has the lowest recognition rate due to its relative dielectric constant ranging from 1.5 to 4, partially overlapping with that of wheat. Thus, plastic may be more difficult to be identified than metal in wheat.

In Fig. 19, we can see that as the number of tags increases, the system recognition rate is significantly affected due to data redundancy. However, when only one tag is selected, the amount of data is too small to accurately measure the features of the object to be recognized.

Table 4
Spatial localization success accuracy using heuristic method in wheat.

Object \ Relocating Times	1	2	3	4
$Metal_s$/Metal	98%/100%	\	\	\
$Rock_s$/Rock	88%/88%	92%/94%	\	\
$Clod_s$/Clod	72%/78%	78%/78%	84%/84%	84%/92%
$Plastic_s$/Plastic	70%/70%	74%/78%	76%/ 84%	76% /84%

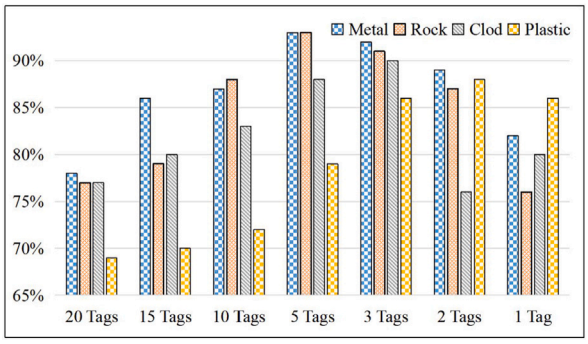

Fig. 19. Recognition accuracy of material properties using different numbers of tag feature vectors.

Therefore, based on Fig. 19, it is more appropriate to use 3 or 5 tags feature vectors with the highest EDR as the model training data.

6. Conclusions

This paper presented TagSee, the first RFID-based system to leverage RFID phase and RSS as feature vectors for foreign materials detection, localization and recognition simultaneously. We first introduced a 3D virtual grid to mark the sensing space according to the two RFID tag arrays deployed on the sides of the sensing area, respectively. Then we proposed an EDR algorithm and a heuristic method to sense the foreign objects locations represented in the form of probability. Also, the possible locations were visualized with the heat map. We conducted a large number of practical experiments to show the effectiveness of TagSee in locating different foreign materials in air and wheat, respectively. In addition, TagSee can recognize the types of foreign materials using a multi-class SVM method. Our experimental results illustrated that TagSee could achieve recognition accuracy of over 86% for four the objects.

CRediT authorship contribution statement

Erbo Shen: Data curation, Methodology, Software, Writing – original draft. **Weidong Yang:** Conceptualization, Methodology. **Xuyu Wang:** Investigation, Methodology, Resources, Writing – review & editing. **Shiwen Mao:** Supervision, Validation.

Declaration of competing interest

The authors declare that they have no known competing financial interests or personal relationships that could have appeared to influence the work reported in this paper.

Data availability

Data will be made available on request.

Acknowledgments

This work is supported in part by the National Science Foundation of Henan, China (No. 222300420004) and Major Public Welfare Special Projects of Henan Province (No. 201300210100), NSFC (No. 62172141, 61772173, 61741107), and Key scientific Research Projects of Colleges and Universities in Henan Province, China in 2022 (22B520021).

References

[1] D. Vasisht, Z. Kapetanovic, J. Won, X. Jin, R. Chandra, S. Sinha, A. Kapoor, M. Sudarshan, S. Stratman, FarmBeats: An IoT platform for Data-Driven agriculture, in: Proc. USENIX NSDI'17, USENIX Association, Boston, MA, 2017, pp. 515–529.
[2] C. Yang, X. Wang, S. Mao, RFID tag localization with a sparse tag array, IEEE Internet Things J. 9 (18) (2022) 16976–16989.
[3] L.M. Ni, Y. Liu, Y.C. Lau, A.P. Patil, LANDMARC: Indoor location sensing using active RFID, in: Proc. IEEE PerCom'03, Fort Worth, TX, Mar., 2003, pp. 701–710.
[4] K. Chawla, C. Mcfarland, G. Robins, W. Thomason, An accurate real-time RFID-based location system, Int. J. Radio Freq. Identif. Technol. Appl. 5 (1) (2018) 48–76.
[5] L. Yang, Y. Chen, X.-Y. Li, C. Xiao, M. Li, Y. Liu, Tagoram: Real-time tracking of mobile RFID tags to high precision using COTS devices, in: Proc. ACM MobiCom'14, Maui, HI, Sept., 2014, pp. 237–248.
[6] J. Wang, J. Xiong, X. Chen, H. Jiang, R.K. Balan, D. Fang, TagScan: Simultaneous target imaging and material identification with commodity RFID devices, in: Proc. ACM MobiCom'17, Snowbird, UT, Oct., 2017, pp. 288–300.
[7] B. Xie, J. Xiong, X. Chen, E. Chai, L. Li, Z. Tang, D. Fang, Tagtag: Material sensing with commodity RFID, in: Proc. ACM SenSys'19, New York, NY, Nov., 2019, pp. 338–350.
[8] C. Yang, X. Wang, S. Mao, TARF: Technology-agnostic RF sensing for human activity recognition, IEEE J. Biomed. Health Inf. 27 (2) (2023) 636–647.
[9] C. Yang, X. Wang, S. Mao, RFID-Pose: Vision-aided 3D human pose estimation with RFID, IEEE Trans. Reliab. 70 (3) (2021) 1218–1231.
[10] C. Yang, Z. Wang, S. Mao, RFPose-GAN: Data augmentation for RFID based 3D human pose tracking, in: The 12th IEEE International Conference on RFID Technology and Applications, RFID-TA'22, Cagliari, Italy, Sept., 2022, pp. 138–141.
[11] E. Shen, W. Yang, X. Wang, S. Mao, W. Bin, TagSense: Robust wheat moisture and temperature sensing using a passive RFID tag, in: Proc. IEEE ICC'22, Seoul, South Korea, 2022, pp. 1617–1622.
[12] M. Sabina, O. Cecilia, N. Shankar, C. Alexandro, N. Corrado Di, M. Gaetano, Humidity sensing by polymer-loaded UHF RFID antennas, IEEE Sens. J. 12 (9) (2021) 2851–2858.
[13] C. Yang, X. Wang, S. Mao, Respiration monitoring with RFID in driving environments, IEEE J. Sel. Areas Commun. 39 (2) (2020) 500–512.
[14] W. Shuaieb, G. Oguntala, A. AlAbdullah, H. Obeidat, R. Asif, R.A. Abd-Alhameed, M.S. Bin-Melha, C. Kara-Zaïtri, Rfid rss fingerprinting system for wearable human activity recognition, Future Internet 12 (2) (2020) 1–12.
[15] K. Ali, A.X. Liu, E. Chai, K. Sundaresan, Monitoring browsing behavior of customers in retail stores via rfid imaging, IEEE Trans. Mob. Comput. (3) (2022) 1034–1048.
[16] B. Zhu, J. Wang, S. Liu, M. Dong, Y. Jia, L. Tian, C. Su, Rfmonitor: Monitoring smoking behavior of minors using cots rfid devices, Comput. Commun. 185 (2022) 55–65.
[17] F.T. Zohra, S. Dey, O. Salim, H. Masoumi, N. Karmakar, Design and analysis of a uhf rfid crack sensor for health monitoring of mining conveyor belt, in: 2020 27th International Conference on Telecommunications, ICT, IEEE, Bali, Indonesia, 2020, pp. 1–5.
[18] A. Abuelkhail, U. Baroudi, M. Raad, T. Sheltami, Internet of things for healthcare monitoring applications based on RFID clustering scheme, Wirel. Netw. 27 (2021) 747–763.
[19] X. Hu, K. Naya, P. Li, T. Miyazaki, K. Wang, Y. Sun, Non-invasive sleeping posture recognition and body movement detection based on rfid, in: 2018 IEEE International Conference on Internet of Things (IThings) and IEEE Green Computing and Communications (GreenCom) and IEEE Cyber, Physical and Social Computing (CPSCom) and IEEE Smart Data, SmartData, IEEE, Halifax, NS, Canada, 2018, pp. 1817–1820.

[20] C. Yang, X. Wang, S. Mao, Rfid-based 3d human pose tracking: A subject generalization approach, Digit. Users Digit. Commun. 008 (003) (2022) 11.
[21] B. Campagne, A. Blouin, L. Pujol, J.P. Monchalin, Compact and fast response ultrasonic detection device based on two-wave mixing in a gallium arsenide photorefractive crystal, Rev. Sci. Instrum. 72 (5) (2001) 2478–2482.
[22] C.B. Lai, B. Xin, W.Q. Chen, L. Rui-Guo, W.U. Shao-Jie, Reason analysis on defects of low alloy steel medium plate by ultrasonic detection, Phys. Exam. Test. 2008 (01) (2008) 44–47.
[23] H. Inoue, Detection of iron k-emission lines from low-mass binary x-ray sources, in: X-ray Astronomy, Astron.Soc.Japan, University of Leicester U.K., 1985, pp. 761–767.
[24] J.W. Pflugrath, The finer things in x-ray diffraction data collection, Acta Crystallogr. D 55 (10) (1999) 1718–1725.
[25] S.A. Durrani, R.K. Bull, Solid state nuclear track detection, Nucl. Tracks 4 (3) (1987) 307–407.
[26] G.F. Knoll, Nuclear radiation detection devices, in: R.A. Meyers (Ed.), Encyclopedia of Physical Science and Technology, third ed., Academic Press, New York, 2003, pp. 763–773.
[27] L.G. Stolarczyk, R. Troublefield, J. Battis, Detection of underground tunnels with a synchronized electromagnetic wave gradiometer, Proc. SPIE - Int. Soc. Opt. Eng. 48 (3) (2005) 10.
[28] Z. Xiang, J. Wu, C. Qi, X. Hu, Contactless detection of moisture content in blended fabrics with a free-space microwave method, IEEE Trans. Instrum. Meas. 69 (5) (2020) 2139–2144.
[29] X. Wang, X. Wang, S. Mao, RF sensing in the internet of things: A general deep learning framework, IEEE Commun. Mag. 56 (9) (2018) 62–67.
[30] Y.U. Yan, L.I. Hong-Wei, O.U. Jin-Ping, Software design and realization of the wireless sensing network applied to structure acceleration monitoring, Appl. Res. Comput. 22 (2) (2005) 197–199.
[31] Y. Ma, N. Selby, F. Adib, Minding the billions: Ultra-wideband localization for deployed rfid tags, in: Proceedings of the 23rd Annual International Conference on Mobile Computing and Networking, in: MobiCom '17, Association for Computing Machinery, New York, NY, USA, 2017, pp. 248–260, http://dx.doi.org/10.1145/3117811.3117833.
[32] E.L. Gomes, M. Fonseca, A.E. Lazzaretti, A. Munaretto, C. Guerber, Clustering and hierarchical classification for high-precision rfid indoor location systems, IEEE Sens. J. 22 (6) (2022) 5141–5149.
[33] J.Y. Shi, X.L. Qin, N. Wang, Rfid indoor symbolic localization algorithm based on strategy of perception ruleset in constrained space, Comput. Sci. 10 (43) (2016) 81–86.
[34] S. Einavipour, R. Javidan, An intelligent IoT-based positioning system for theme parks, J. Supercomput. 77 (6) (2022) 9879–9904.
[35] M. Kim, D. Han, J.K. Rhee, Multiview variational deep learning with application to practical indoor localization, IEEE Internet Things J. PP (99) (2021) 1.
[36] J. Wang, J. Xiong, X. Chen, H. Jiang, D. Fang, Simultaneous material identification and target imaging with commodity RFID devices, IEEE Trans. Mob. Comput. PP (99) (2019) 1.
[37] T. Baranidharan, S. Abipriya, C. Jeyakanthaselvan, D. Suganya, L. Venkataprakash, Health monitoring using internet of things, in: 2017 8th Annual Industrial Automation and Electromechanical Engineering Conference, IEMECON, IEEE, Bangkok, Thailand, 2017, pp. 69–73.
[38] J. Siden, X. Zeng, T. Unander, A. Koptyug, H.E. Nelson, Remote moisture sensing utilizing ordinary RFID tags, in: 2007 IEEE Sensors, Atlanta, GA, 2007, pp. 308–311.
[39] P.K. Singh, N. Kumar, B.K. Gupta, Wireless sensing with radio frequency identification (rfid): Instrumental in intelligent tracking, in: P.K. Singh, Y. Singh, M.H. Kolekar, A.K. Kar, J.K. Chhabra, A. Sen (Eds.), Recent Innovations in Computing, Springer, Singapore, 2021, pp. 345–356.
[40] P. Yang, Y. Feng, J. Xiong, Z. Chen, X.-Y. Li, Rf-ear: Contactless multi-device vibration sensing and identification using COTS RFID, in: IEEE INFOCOM 2020 - IEEE Conference on Computer Communications, IEEE, Beijing, China, 2020, pp. 297–306.
[41] D. Zhong, F. Liu, RF-OSFBLS: An RFID reader-fault-adaptive localization system based on online sequential fuzzy broad learning system, Neurocomputing 390 (2020) (2020) 28–39.
[42] P. Avaltroni, S. Nappi, G. Marrocco, Orthopedic fixture-integrated RFID temperature sensor for the monitoring of deep inflammations, in: 2021 IEEE International Conference on RFID, RFID, IEEE, Atlanta, GA, USA, 2021, pp. 1–6.
[43] S. Einavipour, R.J. Avidan, An intelligent IoT-based positioning system for theme parks, J. Supercomput. 77 (2021) 9879–9904.
[44] D. Wu, D. Zhang, C. Xu, Y. Wang, H. Wang, Widir: Walking direction estimation using wireless signals, in: Proceedings of the 2016 ACM International Joint Conference on Pervasive and Ubiquitous Computing, in: UbiComp '16, Association for Computing Machinery, New York, NY, USA, 2016, pp. 351–362, http://dx.doi.org/10.1145/2971648.2971658.
[45] L. Zhao, Q. Yang, H. Huang, L. Guo, S. Jiang, Intelligent wireless sensing driven metaverse: A survey, Comput. Commun. 214 (2024) 46–56.
[46] B. Hu, H. Peng, Z. Sun, Landmarc localization algorithm based on weight optimization, Chin. J. Electron. 27 (6) (2018) 1291–1296.
[47] F. Liu, D. Zhong, Gsos-elm: An rfid-based indoor localization system using gso method and semi-supervised online sequential elm, Sensors (Basel Switzerland) 18 (7) (2018) 1995–2013.
[48] F.U. Yulu, H. Zhang, R. Liu, G. Liang, H.E. Jing, H. Zhang, Y. Xiao, Fast dynamic object localization fusing with rfid phase and laser, Comput. Eng. 08 (44) (2018) 308–314.
[49] L.X. Qiu, Z.Q. Huang, L.I. Da, 3D tag location aware scheme based on phase interferometric for rfid applications, Chinese J. Comput. 11 (42) (2019) 2512–2525.
[50] E. Rigall, X. Wang, S. Zhang, J. Dong, A fast and accurate rfid tag positioning method based on aoa hologram and hashtables, Comput. Commun. 202 (2023) 135–144.
[51] L. xiangyang, Contactless Intelligent Tracking and Material Perception Recognition Technology Based on Commercial Rfid Equipment (Master's thesis), China University of Science and Technology, 2020.
[52] J. Wang, D. Katabi, Dude, where's my card? rfid positioning that works with multipath and non-line of sight, in: Proceedings of the ACM SIGCOMM 2013 Conference on SIGCOMM, SIGCOMM '13, Association for Computing Machinery, New York, NY, USA, 2013, pp. 51–62.
[53] H. Safa, W. El-Hajj, C. Meguerditchian, A distributed multi-channel reader anti-collision algorithm for rfid environments, Comput. Commun. 64 (2015) 44–56.
[54] H. Yigang, X. Peiliang, z. Lei, C. Chaoqun, Study on frequency shift in mutual coupling effect of ultra-high-frequency radio frequency identification near-field system, J. Electron. Inf. 41 (3) (2019) 9.
[55] W. Hui, Z. Weiwei, S. Yu, Analysis of influencing factors of phase measurement method based on rfid, Electron. Meas. Technol. 41 (5) (2018) 10.
[56] X. Wang, L. Gao, S. Mao, S. Pandey, Csi-based fingerprinting for indoor localization: A deep learning approach, IEEE Trans. Veh. Technol. 66 (1) (2016) 763–776.
[57] C.C. Chang, C.J. Lin, LIBSVM: A library for support vector machines, ACM Trans. Intell. Syst. Technol. 2 (3) (2007) 1–27.